Journal of Luminescence 239 (2021) 118334

Contents lists available at ScienceDirect

Journal of Luminescence

journal homepage: www.elsevier.com/locate/jlumin

On the deconvolution of promptly measured luminescence signals in feldspars

Vasilis Pagonis [a,*], Nathan D. Brown [b], Jun Peng [c], George Kitis [d], George S. Polymeris [e]

[a] McDaniel College, Physics Department, Westminster, MD, 21157, USA
[b] University of Texas at Arlington, Department of Earth and Environmental Sciences, Arlington, TX, USA
[c] Cold and Arid Regions Environmental and Engineering Research Institute, Chinese Academy of Sciences, Lanzhou, 730000, China
[d] Aristotle University of Thessaloniki, Physics Department, Nuclear Physics and Elementary Particles Physics Section, 54124, Thessaloniki, Greece
[e] Institute of Nanoscience and Nanotechnology, NCSR Demokritos, Ag. Paraskevi, 15310, Athens, Greece

ARTICLE INFO

Keywords:
Luminescence
Feldspar
Tunneling
R
OSL
IRSL
TL
Thermochronometry

ABSTRACT

Thermally and optically stimulated luminescence signals from feldspars have been the subject of numerous experimental and modeling studies, due to the importance of these signals in luminescence dosimetry and luminescence dating. Despite these extensive previous studies, there are no standardized computerized deconvolution methods for analyzing these signals in the literature. In this paper we present a simple and consistent method which can be used to perform computerized deconvolution of thermoluminescence (TL), continuous-wave infrared stimulated luminescence (CW-IRSL) and linearly-modulated (LM-IRSL) signals from feldspars. The method can be used with promptly measured luminescence signals from laboratory irradiated samples. R scripts are used in several examples to carry out the deconvolution of TL, CW-IRSL and LM-IRSL luminescence signals from different types of feldspars, including K feldspars extracted from bedrock and from a suite of geological museum samples. The results of the analysis show that the TL glow curves can be described in a uniform manner, as the superposition of several components corresponding to different activation energies. All TL, CW-IRSL and LM-IRSL signals can be described by a narrow range of the dimensionless acceptor density parameter, consistent with previous analysis of these luminescence signals in the literature, which have concluded that these luminescence signals are likely to share a common recombination center.

1. Introduction

Thermally and optically stimulated Luminescence signals from feldspars have been the subject of numerous experimental and modeling studies, due to the importance of these signals in luminescence dosimetry and luminescence dating. Despite these extensive previous studies, there are no standardized computerized methods of analyzing these signals in the literature.

Recently Pagonis et al. [1] presented open-access R scripts Feldspar Simulation Functions (FSF), for kinetic model simulation of luminescence phenomena in feldspars. The key physical concept of the FSF is that irradiation and thermal/optical treatments of feldspars change the distribution of nearest neighbor (NN) distances in donor-acceptor pairs. These authors presented practical examples of using the FSF to analyze *single component* thermoluminescence (TL) and continuous-wave infrared stimulated luminescence (CW-IRSL) signals, in order to extract the physical parameters characterizing the feldspar samples.

This paper extends the work of Pagonis et al. [1], by presenting computerized deconvolution of *multi-component* TL, CW-IRSL and linearly-modulated IRSL (LM-IRSL) signals from feldspars.

The specific goals of the paper are:

- To develop R scripts for the deconvolution of TL, CW-IRSL and LM-IRSL signals containing several components. The scripts are based on the approximate analytical solutions developed by Kitis and Pagonis [2], within the excited state tunneling model (EST) developed by Jain et al. [3]. These analytical solutions apply for promptly measured luminescence signals from laboratory irradiated samples.
- To describe luminescence signals from a wide variety of feldspars of different geological provenance, and to look for common characteristics in the numerical parameters extracted using the EST model.

* Corresponding author.
E-mail address: vpagonis@mcdaniel.edu (V. Pagonis).

https://doi.org/10.1016/j.jlumin.2021.118334
Received 30 May 2021; Received in revised form 5 July 2021; Accepted 7 July 2021
Available online 13 July 2021

- To investigate whether the three luminescence signals from the same feldspar sample can be described consistently, by using a common set of model parameters.

2. Samples and experimental protocols

2.1. The suite of museum feldspars studied by Polymeris et al. [4]

The luminescence signals from the feldspar samples used in this paper have been studied initially by Polymeris et al. [4] and more recently by Sfampa et al. ([5,6]).

In very general terms, the basic structure of an alkali feldspar consists of a three dimensional array of corner-sharing AlO_4 and SiO_4 tetrahedra. Three out of the four T cation sites in the unit cell are occupied by a Si-cation, and the fourth by an Al-cation. For example, the high temperature form of KAlSi3O8 is termed a sanidine and is monoclinic. The structure of sanidines contains two distinct Si/Al tetrahedral sites, denoted by T^1 and T^2. By contrast, microclines are the low temperature form and the unit cell is triclinic, with highly ordered distribution of Al/Si cations among four distinguishable tetrahedral sites, denoted by T^1(o), T^2(o), T^1(m) and T^2(m). Orthoclase is considered an intermediate form between sanidine and microcline. Using XRD studies Polymeris et al. [4] characterized the structural parameters of the 10 feldspars, by using the probability of the Al-cation to occupy the T1 sites and also by measuring the volume of the unit cell. This group of museum samples contains sanidines, orthoclases and microclines (see Polymeris et al. [4], their Table 1). The K-feldspars were separated from mafic and felsic minerals with the use of Franz (model L-1) magnetic separator and Sodium Polytungstate (SPT) heavy liquid, respectively. X-ray powder diffraction (XRPD) were used in order to identify the purity of K-feldspars, to estimate the unit cell parameters, and to classify the samples by calculating the probability of an Al cation occupying one of the T1 sites.

These authors found a good correlation between the TL sensitivity and individual K feldspar structure, and suggested that these samples are ideal for investigating basic thermally and optically stimulated signals (TL, IRSL etc).

The TL measurements for these feldspar samples were carried out using a Risø TL/OSL reader (model TL/OSL-DA-15), equipped with $^{90}Sr/^{90}Y$ beta particle source, delivering a nominal dose rate of 0.105 Gy/s. A 9635QA photomultiplier tube with a combination of Pilkington CA-3 heat absorbing and a Corning blue filter was used for light detection. All measurements were performed with low constant heating rates of 1 K/s in order to avoid significant temperature lag, and the samples were heated up to the maximum temperatures of 500 °C. The grain size of the samples was 90–150 μm.

In the experimental protocol for measurement of the TL glow curves, an aliquot of the material is irradiated with a dose of either 10 Gy or 40 Gy, followed by a measurement of the TL signal by heating up to 500 °C with a constant heating rate of 1 K/s. The possibility of sensitivity changes which may occur during repeated heating and irradiation were tested during this experimental protocol, by measuring the TL signals before and after the end of the protocol. It was found that the reproducibility of the signals was better than 2%, indicating that there was no need for sensitivity corrections in these experiments.

Typical results for the TL glow curves of the samples by Polymeris et al. [4] are shown in Fig. 1, for an irradiation dose of 40 Gy. The TL signals were normalized to the maximum TL intensity, and they exhibit a wide range of shapes, with apparent maximum TL intensities at several temperatures between room temperatures and 500 °C. The TL signals were measured immediately after the end of the irradiation process.

Table 1
List of the 10 K-Feldspar samples studied by Polymeris et al. [4], Sfampa et al. [5].

Sample No	Lab. Code name	K-Feldspar species
1	BAL2	Sanidine
2	SAM2	Sanidine
3	SAM3	Sanidine
4	MRK4	Orthoclase
5	XAN8	Orthoclase
6	VRS4	Orthoclase
7	ELD1	Microcline
8	VRS3	Microcline
9	VRS8	Microcline
10	KST4	Microcline

2.2. The bedrock samples studied by Brown et al. ([7,8])

A second set of feldspar samples measured in this study were taken from the tectonically uplifted crustal block known as the Beartooth uplift, located near the town of Red Lodge, Montana, USA. This uplifted region is a 60 × 125 km block of Precambrian crystalline basement which was initially exhumed during the Laramide orogeny, a period of mountain building in the western USA between ~80 to 35 Ma (Wise [9]). Apatite fission-track results from a 2.5-km-deep exploratory well indicate a two-stage uplift history, with the first stage beginning around 61 Ma and resulting in 4–8 km of uplift, and the second stage beginning between 15 and 5 Ma and producing about 4 km of uplift, which continues to the present (i.e., 0.3–0.8 mm/yr) (Omar et al. [10]).

Bedrock samples were detached by sledge hammer and chisel from rock outcrops that seemed to be in place (i.e., not 'float'). The latitude, longitude, and elevations of sample collection locations were measured with a handheld GPS system. After sample collection, the bedrock samples were spray-painted with a contrasting color and then broken into smaller pieces under dim amber LED lighting in the laboratory. The sunlight-exposed, outer-surface portions of the samples were separated from the inner portions.

The unexposed inner portions from the samples were then crushed by hand using a pestle and mortar and sieved to isolate the 175–400 μm size fraction. These separates were then treated with 3% hydrochloric acid and separated by density using lithium metatungstate heavy liquid ($\rho <$ 2.565 g/cm^3; Rhodes [11]) in order to isolate the most potassic feldspar grains. Grains were mounted on stainless steel discs in a small-diameter (3–5 mm) monolayer using silicon oil. No hydrofluoric acid was used to etch these crystals.

All luminescence measurements were performed at the UCLA luminescence laboratory using a TL-DA-20 Risø automated reader equipped

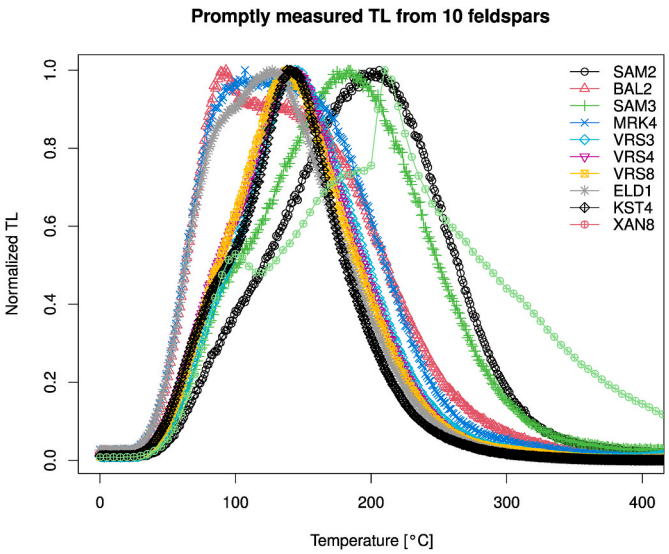

Fig. 1. Typical promptly measured TL signals from the suite of feldspars studied by Polymeris et al. [4]. The signals have been normalized to the maximum TL intensity and the regenerative dose was 40 Gy.

with a $^{90}Sr/^{90}Y$ beta source which delivers 0.1 Gy/s at the sample location (Bøtter-Jensen et al. [12]). Emissions were detected through a Schott BG39 filter combination (transmitting between ~325–475 nm), thermoluminescence measurements were performed in a nitrogen atmosphere and glow curves were measured at a heating rate of 5 °C/s.

A total of 12 samples were studied and analyzed, and these are listed in Table 3. The TL signal of two aliquots from each sample were measured, for a total of N = 24 TL glow curves. The samples were given a dose of 5 Gy, and a delay of 100 s was introduced before measurement of the TL glow curves, in order to avoid a phosphorescence signal present at room temperature immediately after the irradiation process. It is noted that such a phosphorescence signal was not observed for the museum feldspar samples of Polymeris et al. [4]. The thermal background was then measured and subtracted from each glow curve. In some of the samples, CW- and LM-IRSL shine-down curves were measured at 50 °C for 100 s, following a beta dose of 1.2 kGy and a preheat to 250 °C for 60 s.

3. Quantum tunneling from the excited state of the electron trap

During the past decade significant progress has been made both experimentally and theoretically in understanding the behavior of luminescence signals from feldspars, apatites and other natural materials. Quantum mechanical tunneling and the associated phenomenon of "anomalous fading" of these luminescence signals are now well established as dominant mechanisms in these materials (for a recent overview see for example Pagonis et al. [13]). From a modeling point of view, one considers a random distribution of electrons and acceptors in a crystal, and introduces the concept of the distribution of nearest neighbor distances.

In a recent paper, Pagonis et al. [1] discussed in detail the excited state tunneling (EST) model of Jain et al. [3], and presented open access R codes for the analysis of TL glow curves in feldspars. The EST model and the R codes are also discussed in some detail in the recent book by Pagonis [14]. Specifically these authors discussed how the promptly measured TL signals from laboratory irradiated feldspars can be analyzed using the following analytical equation for the intensity of a TL signal (see equations (29) and (30) in Kitis and Pagonis [2]):

$$I_{TL}(t) = \frac{I_0\, F(t)^2\, e^{-\rho' (F(t))^3} \left(E^2 - 6k_B^2 T^2\right)}{E k_B s T^2 z - 2k_B^2 s T^3 z + \exp(E/k_B T) E\beta} + bgd \tag{1}$$

$$F_{TL}(t) = \ln\left(1 + \frac{z\, s\, k_B T^2}{\beta E}\, e^{-\frac{E}{k_B T}} \left(1 - \frac{2k_B T}{E}\right)\right) \tag{2}$$

where s (s^{-1}) is an effective frequency parameter characterizing the TL process, T (K) is the temperature of the sample, E (eV) is the thermal activation energy of the trap, $z = 1.8$ is a constant in the model, k_B (eV K^{-1}) is the Boltzmann constant, β (K/s) is the constant heating rate and I_0 (a.u.) is a scaling constant. This analytical equation is used throughout this paper to analyze complex TL glow curves, and was termed the *KP-TL equation* by Pagonis et al. [1].

The fitting parameters in the least squares deconvolution procedure for TL signals using Eqs. (1) and (2) are I_0, E, s, ρ', bgd. Even though the above equations look rather complex, they are easy to code.

Pagonis et al. [1] also presented open access R codes for the analysis of CW-IRSL signals in feldspars. Specifically these authors discussed how experimental CW-IRSL data can be analyzed using the following analytical equation, which was termed the *KP-CW equation* by Pagonis et al. [1]:

$$I_{CW-IRSL}(t) = \frac{I_0\, F(t)^2\, e^{-\rho' (F(t))^3}}{1 + zA\, t} + bgd \tag{3}$$

$$F_{CW-IRSL}(t) = \ln(1 + zA\, t) \tag{4}$$

where the rate of optical excitation A **(s^{-1})** is given by $A = \sigma I$, where σ (cm^2) represents the optical cross section for the process, and I ($cm^{-2}s^{-1}$) is the intensity of the excitation IR source. It is notedthat Pagonis et al. [1] used Eqs. (3) and (4) with the constant zA replaced by a constant A, while in this paper we use these equations with z = 1.8, in order to be consistent with the notation of the equations for TL and LM-IRSL presented in this section.

The fitting parameters in the deconvolution process for CW-IRSL signals using Eqs. (3) and (4) are A, I_0, ρ' and a constant background *bgd*. Several experimental studies have found that typical values of the infrared stimulation rate A are 1–10 s^{-1}, and that for CW-IRSL and TL signals in feldspars the typical values of the dimensionless density $\rho' =$ 0.003–0.02 (see for example the comprehensive studies by Pagonis et al. [15], Sfampa et al. [5,16], Kitis et al. [17] and Sahiner et al. [18]).

In this paper we also analyze LM-IRSL curves, using the following analytical equation, which is termed hereby the *KP-LM equation* (see equation (25) in Kitis and Pagonis [2]):

$$I_{LM-IRSL}(t) = \frac{I_0\, F(t)^2\, e^{-\rho' (F(t))^3}}{1 + zb\, \frac{t^2}{2P}} + bgd \tag{5}$$

$$F_{LM-IRSL}(t) = \ln\left(1 + zb\, \frac{t^2}{2P}\right) \tag{6}$$

where P **(s)** is the total stimulation time during the LM-IRSL experiment and b is the rate of optical excitation in s^{-1}. The fitting parameters in the deconvolution process of LM-IRSL signals using Eqs. (5) and (6) are b, I_0, ρ' and a constant background *bgd*.

In this paper we carry out deconvolution of the complex TL glow curves by using the KP-TL, KP-CW and KP-LM Eqs. (1), (3) and (5) respectively. While in the recent work of Pagonis et al. [1] these equations were used to fit experimental data from single component TL and CW-IRSL signals, in this paper the equations are used to describe signals consisting of *several* components.

The analysis is based on the following physical assumptions, which were previously summarized in Pagonis et al. [19]: (a) The promptly measured luminescence signal from a laboratory irradiated sample consists of several constituent glow peaks, each corresponding to a different population of donor-acceptor (d-a) pairs. The d-a pairs for each component in the signal are randomly distributed, and each component in the irradiated sample is described by its own symmetric nearest neighbor distribution. (b) There are many more acceptors in the material than donors, so that the material is characterized by a constant acceptor density parameter ρ'. Electrons from the various components are likely to be accessing the same recombination center, and all components are characterized by the same constant parameter ρ'.

An important question concerning the deconvolution of feldspar TL is under what experimental conditions one can use the KP-equations presented in this section. This is considered further in the Discussion section of this paper.

4. Experimental results for the suite of feldspars studied by Polymeris et al. [4]

In this section we present the results of the TL deconvolution of the 10 feldspars studied by Polymeris et al. [4]. In order to constrain the least squares fitting method, the activation energies E are determined by using the fractional glow technique, as described in section 4.1. These experimentally determined E values are used as the starting parameters to carry out the deconvolution least squares fittings to the experimental data. Section 4.2 presents the method used to decide on the optimal number of components N in the TL signal, and section 4.3 presents the deconvolution results for the 10 feldspar samples. Finally, in section 4.4 the parameters from the TL deconvolution analysis are compared with the previous study of these samples by Sfampa et al. [5].

4.1. Results from the fractional glow (FG) technique

As a first step in the analysis of the complex TL glow curves in these samples, the well-known fractional glow (FG) technique is applied, with typical results shown in Fig. 2 for microcline sample ELD1. A detailed discussion of these FG results was given in Pagonis et al. [19]. In the fractional glow technique, the activation energy E of the traps is evaluated by thermal removal of lower temperature peaks, and the sample is heated and cooled several times. For each cycle one applies the initial rise method, and the resulting activation energy E is plotted as a function of the temperature, forming a step-like graph. Pagonis et al. [19] used quantitative criteria in interpreting the data in Fig. 2 as a series of at least five distinct energy levels, located approximately at $E = 0.8$, 0.95, 1.15, 1.25, 1.40 eV. These E values are used as initial starting values for the deconvolution process which fits the TL glow curves with the sum of components using Eq. (1). The optimal E values are obtained by small adjustments to the above values during the fitting of the TL glow curves, by allowing a random ±10% variation in all E values.

It is important to note that the FG results are only a first (but necessary) step in the deconvolution process, since they provide a first approximate estimate of the E values and of the possible number of components N in the TL signal. A second and more important step in the deconvolution is to introduce quantitative numerical criteria which will allow a more accurate estimate of the number of components N and of their corresponding E values. This process of estimating the N and E values is described in the next subsection.

The *physical* interpretation of FG results similar to Fig. 2 in feldspars has been a re-occurring research question. For example, one of the fundamental questions is whether one is dealing with a continuous distribution of energies E, with a continuous distribution of frequency factors s, or perhaps even with a combination of both possibilities. This important question is discussed in some detail in the *Appendix* of this paper, by using the physical description in the model of random defects by Jain et al. ([3,20]).

4.2. Deciding the optimal number of components N

The next step in the deconvolution process is to determine the optimal number of components N required to fit the TL glow curves.

The analysis of complex TL glow curves is complicated by the fact that the exact number of overlapping peaks is unknown. Basically, the process of curve fitting consists of a first guess of the parameters, evaluating the TL glow curve using this set of parameters, and comparing it to the experimental curve. The parameters are then changed so that the difference between the experimental and calculated curves is minimized. A popular way of doing this is the Levenberg-Marquardt nonlinear least-squares fitting procedure which minimizes the *objective function*:

$$f = \sum_{i=1}^{n} \left(y_i^{expt} - y_i^{fit}\right)^2, \qquad i = 1 \ldots n \tag{7}$$

where y_i^{expt} and y_i^{fit} are the i-th experimental point and the fitted value respectively, and n is the number of data points (see for example Moré [21], and the discussion in the book by Chen and Pagonis [22]).

At the end of the fitting process of minimization of f, one evaluates the goodness of fit of the equation to the data, which is often expressed by the Figure of Merit (FOM) defined as follows (Balian and Eddy [23]):

$$FOM = \frac{\sum_{i=1}^{n} \left|y_i^{expt} - y_i^{fit}\right|}{\sum_{i=1}^{n} \left|y_i^{expt}\right|}, \qquad i = 1 \ldots n \tag{8}$$

Since the *FOM* is normalized by the integral under the curve, the goodness of fit may be compared from one glow curve to another. Fits are usually considered to be acceptable when the *FOM* is of a few percent.

Obviously, one wishes to get a *global minimum* of the objective function f in Eq. (7), in order to obtain the best possible set of parameters. Unfortunately, non-linear functions usually have many *local minima*, and practically all the methods of minimization lead to a local minimum which may not necessarily be global. However, several methods have been used for such minimization and for increasing the probability of approaching the global minimum, even when the initial guess of the set of parameters is rather far from the final optimum (see for example, the detailed study of luminescence data in Bluszcz and Adamiec [24]).

In addition to the FOM, the goodness of fit is also commonly expressed by using the χ^2 parameter, defined often as the weighted (or unweighted) sum of the squares between the experimental and fitted values. For unweighted sets of data, one can use:

$$\chi^2 = \sum_{i=1}^{n} |y_i^{expt} - y_i^{fit}|^2, \qquad i = 1 \ldots n \tag{9}$$

In this paper, the Figure Of Merit (FOM) and χ^2 parameter are used as two quantitative criteria, to decide on the optimal number of components N in a glow curve. The unweighted data is used in our analysis, however the use of weighted data gave very similar results.

In addition to using the FOM and χ^2 criteria, the more complex deconvolution technique suggested by Bluszcz and Adamiec [24] was also used for a few of the TL glow curves, for comparison purposes. These authors suggested an algorithm which successively increases the number of components N until an optimal value of components is reached, based on a statistical F-ratio. This method of deciding the optimal number of components gave similar results with our method of using the FOM and χ^2, however it also gave inconsistent results in some cases, most likely due to the low resolution of our experimental data. After considering the results from all three methods (FOM, χ^2 and F-ratio), it was decided to apply the FOM minimization method to all TL glow curves in this paper.

A typical TL glow curve with $N = 7$ components would be described by a large number of 22 free fitting parameters, namely the energy parameters E_i $(i = 1 \ldots 7)$, the corresponding frequency parameters s_i $(i = 1 \ldots 7)$, the amplitudes of the TL components A_i $(i = 1 \ldots 7)$, and the density parameter ρ'.

Although one can proceed by using 22 fitting parameters in the least squares procedure, it is good practice in such complex situations to attempt a reduction of the number of required fitting parameters, if

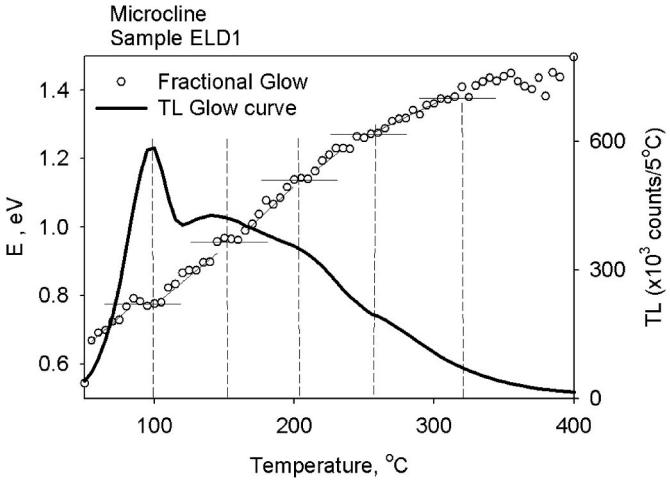

Fig. 2. The fractional glow method applied to microcline sample ELD1, showing the presence of at least five distinct energy levels, located approximately at E = 0.8, 0.95, 1.15, 1.25, 1.40 eV. These E values are used as initial starting values for the deconvolution of the TL glow curves using Eq. (1). Similar results were obtained for the other 9 samples shown in Fig. 1. For a detailed discussion of this set of fractional glow data, see Pagonis et al. [19].

possible. By reducing the number of fitting parameters, it may become easier and more efficient for the least squares routines to reach a local or global minimum. For example, in a detailed study of continuous distributions in persistent phosphors, De Clercq et al. [25] used three Gaussian energy distributions to describe the broad TL glow curves in these materials, and assigned the *same* frequency factor s to all three distributions. These authors recommended using a common s-value for the three distributions, because the s and corresponding E values are highly correlated.

By following the suggestion by De Clercq et al. [25], we assign the same s value for each of the $N = 7$ components shown in Fig. 3(c). As with any model, we do not claim that assigning this common s value is the "correct" choice, but we use this instead as our working modeling hypothesis; in general, one should consider all possibilities in order to find the optimal number of fitting parameters.

4.3. Results from the deconvolution of TL glow curves for the samples in Table 1

Fig. 3 shows the results of the deconvolution process for microcline sample VRS8. In Fig. 3(a)–(d) the number of components used is $N = 6$, 7, 8, 9 respectively. In each of these cases the values of FOM and χ^2 are evaluated, and are plotted in Fig. 3(e) and (f) correspondingly. Both the FOM and χ^2 values show a minimum for $N = 7$ components in this example, so it was decided that the optimal number of components for this sample is $N = 7$. This procedure is repeated for all ten museum samples shown in Table 1, as well as for the 12 bedrock samples listed in Table 3.

In the example of Fig. 3(c) with $N = 7$, the complex TL glow curve is analyzed as the sum of seven individual peaks, located at approximate temperatures of $T_{max} = 75$, 120, 180, 230, 290, 380, 450 °C.

The R code uses the Levenberg-Marquardt algorithm and the *nlsLM()* function within the R package *minpack* (Moré [21]). This function also allows for constraining the range of parameters in the model. In the example shown in Fig. 3(c), the values of the parameters $E_1 \ldots E_7$ are constrained within ±10% from the starting values of E = 0.80, 0.90, 1.06, 1.19, 1.40, 1.60 eV. The value of the frequency factor is constrained in the range $s = 10^{10} - 10^{14}$ s^{-1}, and the density parameter in the range $\rho' = 0.001$–0.015. The starting values for s, ρ' are $s = 10^{12}$ s^{-1} and $\rho' = 0.01$.

Fig. 4 shows typical results from analyzing 6 of the 10 feldspars studied by Polymeris et al. [4], after an irradiation dose of 40 Gy. Very good fits are obtained for all samples, with the optimal number of components found to be $N = 7$ for 8 out of the 10 feldspars, and with 2 of the samples requiring only $N = 6$ components.

Fig. 5 shows a compilation of the best fit parameters from the deconvolution analysis of all 10 feldspars, using radial plots. We have used the convenient function *plot_RadialPlot()* provided in the R package *Luminescence* (Dietze et al. [26], Bøetter-Jensen et al. [12]).

In a radial plot, the position of each point on the x-axis is a measure of the precision with the quantity is known, in terms of the relative error (expressed as a percentage). The value plotted on the y-axis, is the number of standard deviations that a value lies away from the reference value, taken to be mean value of all data. A third radial axis is used on the right-hand side of the graph, and a band is drawn from the '+2' and '-2' points on the y-axis, denoting the area within which the data will lie

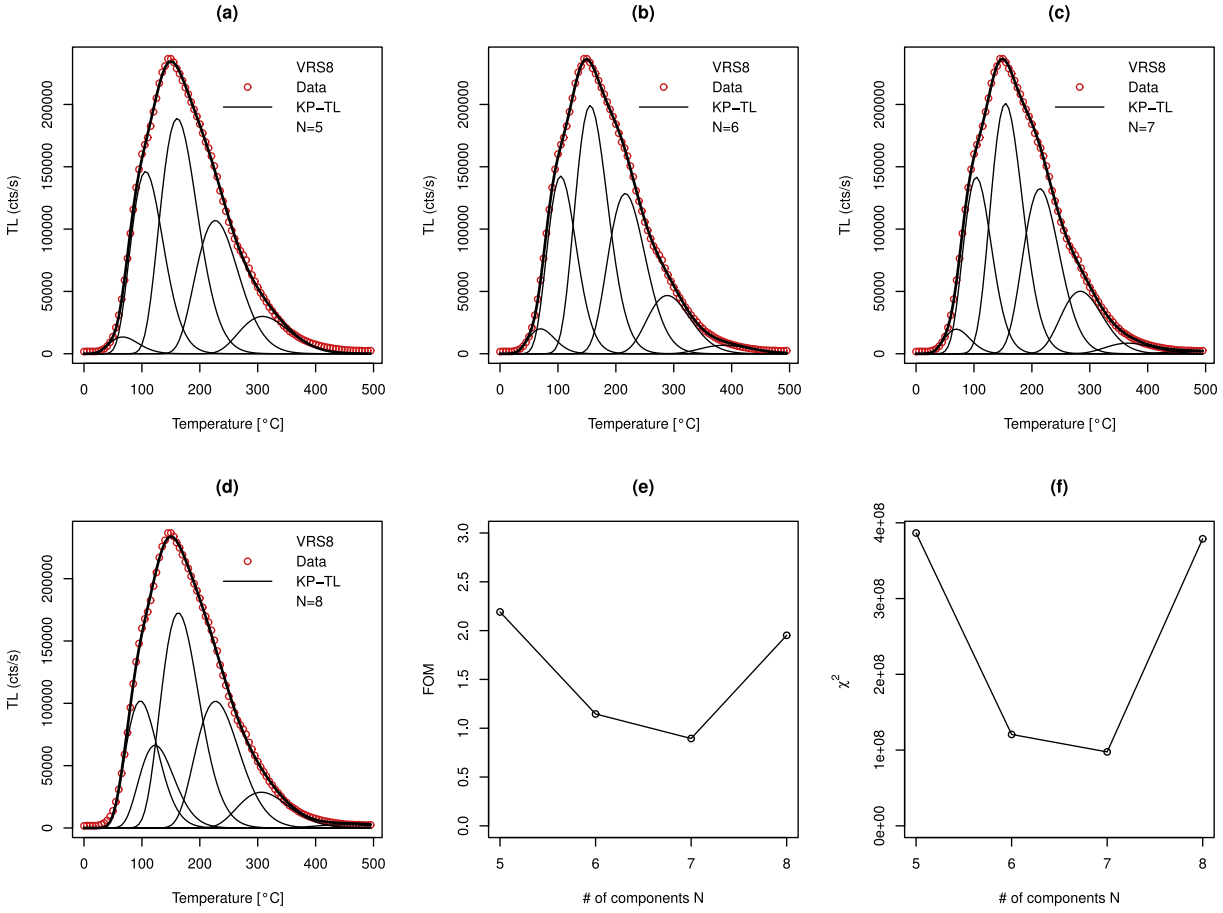

Fig. 3. (a)–(d) Examples of applying the KP-TL equation (1) as a deconvolution function to microcline VRS8, using N = 5,6,7,8 components. (e) The FOM and (f) the χ^2 from the best fits in (a)–(d) as a function of the number of components N. In this example, the best fit is obtained for $N = 7$, corresponding to the minimum of both the FOM and χ^2 graphs.

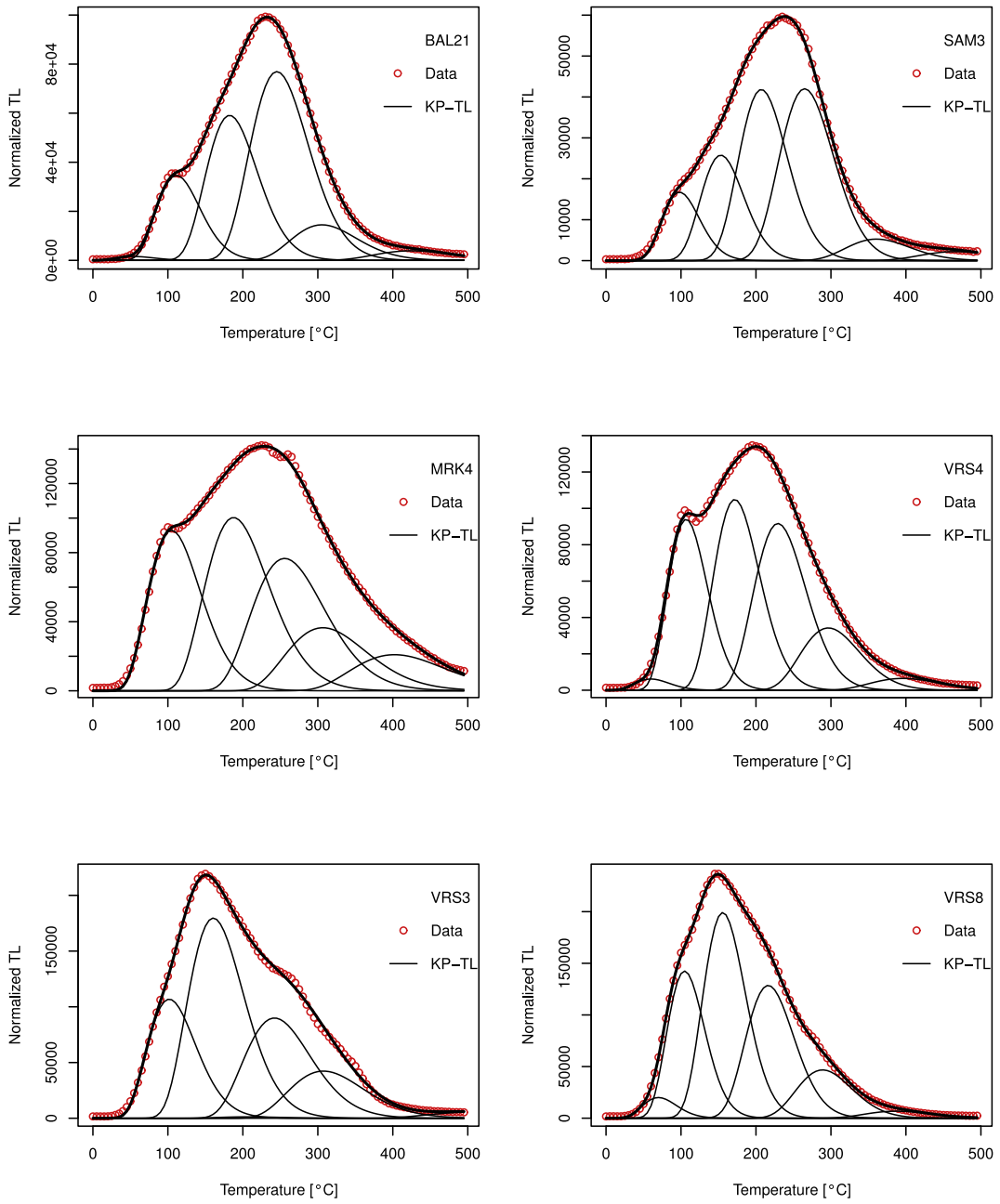

Fig. 4. Examples of the deconvolution of TL glow curves from six of the 10 samples studied by Polymeris et al. [4]. The parameters from the deconvolution analysis for all 10 feldspars are shown in Fig. 5, and the irradiation dose was 40 Gy. All glow curves shown here were fitted with $N = 7$ components, except samples SAM3 and VRS3 which were fitted with $N = 6$.

if they are consistent with a given value of within 2 standard deviations. Thus, for a single population, 95% of the points should fall within this band.

Fig. 5 (a),(b) show the radial plots for the first two activation energy values E_1, E_2, while Fig. 5(c) is the respective radial plot for the 10 ρ' values and Fig. 5(d) is the plot for the frequency factors $ln(s)$. Similar radial plots were obtained for the rest of the activation energy parameters $E_3 \cdots E_7$.

For the samples in Fig. 5(a)–(d), all 10 values fell within the shaded bands. Furthermore, a comparison of the radial plots in Fig. 5 shows that the relative standard errors (RSE) for E_1, E_2, s are much smaller that the corresponding RSE for the dimensionless density parameter ρ'.

We have repeated the analysis indicated in Fig. 4 for a second set of TL glow curves from the same 10 samples, which were irradiated at a lower dose of 10 Gy. Fig. 6 shows a compilation and cross-comparison of the high dose (40 Gy) and low dose (10 Gy) data from the 10 feldspars. The errors bars are the individual standard errors obtained from the least squares fitting procedure. The average value $\rho' = 0.006 \pm 0.002$ of all data is shown as a horizontal *solid* line, and the two horizontal *dashed* lines represent the 95% confidence intervals ($\pm 2\ \sigma$) for the data. It is concluded that the density parameter ρ' is independent of the irradiation dose given to the sample, at least for the doses studied here. It is also noted that the 10 feldspar samples can be described by a narrow range of ρ' values, which is very similar to the narrow range of values $\rho' = 0.002$–0.010 obtained by Pagonis et al. [15], from the analysis of CW-IRSL signals of 23 museum samples of a very different provenance.

In the next subsection, the values of ρ' from the deconvolution of these 10 TL signals will be compared with the detailed study by Sahiner et al. [18].

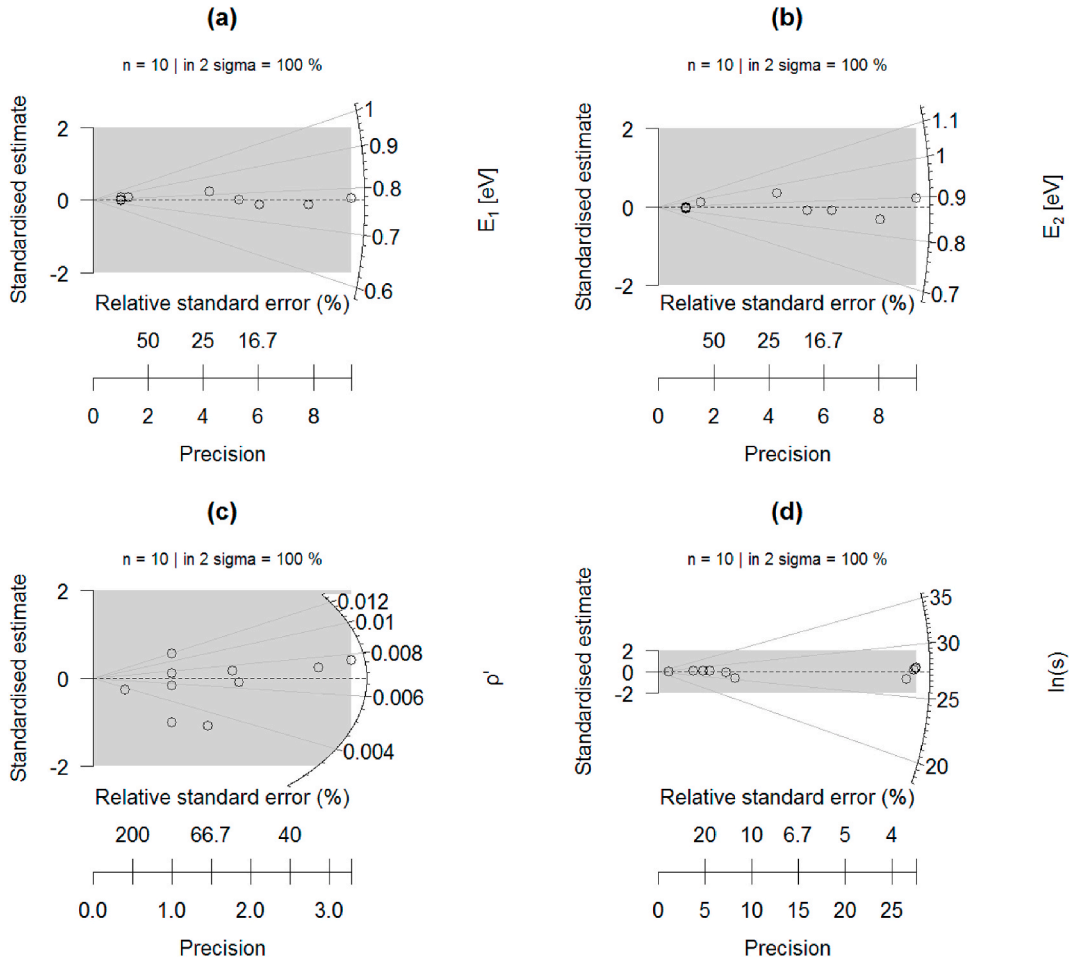

Fig. 5. Radial plots of the best fit parameters obtained from the TL deconvolution analysis of the 10 feldspars by Polymeris et al. [4], fitted using the KP-TL analytical Eq. (1). For more details on the samples, see Brown et al. [7]. (a)–(b) Radial plots of the first two activation energy values E_1, E_2 (c) Radial plot of ρ' values (d) Radial plot of the frequency factors s.

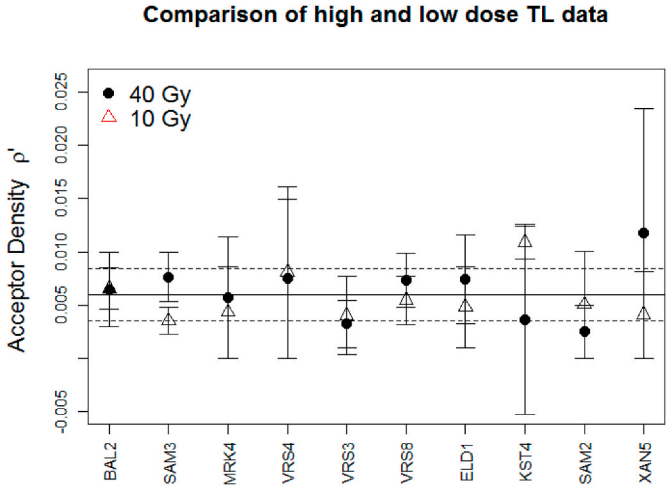

Fig. 6. Plot of ρ' values from TL deconvolution of all 10 feldspars previously studied by Polymeris et al. [4]. The data shown are obtained at two different irradiation doses of 40 Gy and 10 Gy, and the errors bars are the individual standard errors obtained from the least squares fitting procedure. The average ρ' values of all data is shown as a solid horizontal line, and the two dashed horizontal lines represent the 95% confidence intervals ($\pm 2\ \sigma$) for the data.

4.4. Comparison of ρ' values from TL deconvolution, with the analysis of TL and CW-IRSL signals in Sfampa et al. [5]

In this subsection we compare the results from the deconvolution of the TL signals, with the CW-IRSL results obtained by Sfampa et al. [5], for the same 10 feldspars. Table 2 summarizes the results from their detailed study, in which they used the general expressions in the model by Jain et al. [3] to estimate the dimensionless density parameter ρ'.

These authors obtained estimates of ρ' by analyzing the following three independent sets of experimental data:

(a) Fitting the CW-IRSL signals using the KP-CW Eq. (3).
(b) Fitting an analytical equation to the amount of TL lost after exposure of the samples to 850 nm infrared LEDs (CW-IRSL) of various stimulation times.
(c) Fitting an analytical equation to the amount of TL lost after exposure of the samples to 470 nm blue LEDs (OSL) of various stimulation times.

The compiled data from Table 2 are shown as a graph in Fig. 7, with the error bars indicating the standard error in the parameter ρ' resulting from the least squares fit of the TL data in this paper (Fig. 4).

The 4 different sets of experimental data shown in Table 2 and Fig. 7 are in reasonable agreement with each other, at least within the accuracy and precision of the experiments. Furthermore, all ρ' values are within a narrow range previously established in the study by Pagonis et al. [15].

Table 2
List of the density parameter ρ' for the 10 K-Feldspar samples studied by Polymeris et al. [4], obtained by analysis from a variety of signals (Sfampa et al. [5]). The errors shown in the third column are the standard errors obtained from the least squares procedure in this paper.

Sample	Lab. Code	ρ' from TL fits	ρ' from	ρ' from lost TL,	ρ' from lost TL,
Index	Name	(this paper)	CW-IRSL [5]	after IR [5]	after OSL [5]
1	BAL2	0.0064 ±0.0034	0.0018	0.0018	0.0018
2	SAM2	0.0025 ± 0.0025	0.0012	0.0016	0.0016
3	SAM3	0.0076 ± 0.0023	0.0018	0.0015	0.0015
4	MRK4	0.0057 ± 0.0057	0.0035	0.0028	0.0020
5	XAN5	0.012 ± 0.012	0.0024	0.0034	0.0027
6	VRS4	0.0075 ± 0.0075	0.0057	0.0032	0.0034
7	ELD1	0.0074 ± 0.0041	0.0066	0.0042	0.0035
8	VRS3	0.0032 ± 0.0022	0.0042	0.0034	0.0023
9	VRS8	0.0073 ± 0.0026	0.0056	0.0041	0.0033
10	KST4	0.0036 ± 0.0009	0.0024	0.0034	0.0020

Table 3
List of the 12 bedrock samples studied in this paper. For each of these samples, the TL glow curve was measured using two different aliquots, resulting in a total of $M = 24$ measured glow curves. The details of these samples were previously presented in the papers by Brown and Rhodes [7,8].

Sample index	Sample laboratory code	Sample Lithology	Mineralogy of separates
1	J0994	Granitic gneiss	
2	J0995	Tonalitic gneiss	High albite
3	J0996	Dacite porphyry	
4	J0997	Dacite porphyry	
5	J1000	Granodiorite gneiss	
6	J1001	Granitic gneiss	Perthite
7	J1002	Granitic gneiss	
8	J1003	Granitoid gneiss	
9	J1004	Tonalitic gneiss	
10	J1006	Dacite porphyry	
11	J1007	Granitic gneiss	
12	J1010	Granitic gneiss	

5. Deconvolution of TL, CW-IRSL and LM-IRSL signals extracted from bedrock samples

In this section we present the results of the deconvolution of TL, CW-IRSL and LM-IRSL signals from several North American bedrock feldspars, previously described in section 2.2. In section 5.1 the results of the TL deconvolution analysis are presented, while in section 5.2 a deconvolution is carried out for the CW-IRSL signals by using the KP-CW equation. Finally section 5.3 contains an analysis of LM-IRSL signals from three bedrock samples, and also a direct comparison of all three types of signals from the same sample.

5.1. Deconvolution of TL signals extracted from bedrock samples

The deconvolution method presented in the previous sections was next applied to a large number of TL glow curves measured using the bedrock samples studied by Brown et al. ([7,8]). The complete list of 12 samples is given in Tables 3 and 2 aliquots were measured for each sample, resulting in a total of $M = 24$ deconvoluted TL glow curves. The lithology and mineralogy for several of these samples is also shown in Table 3.

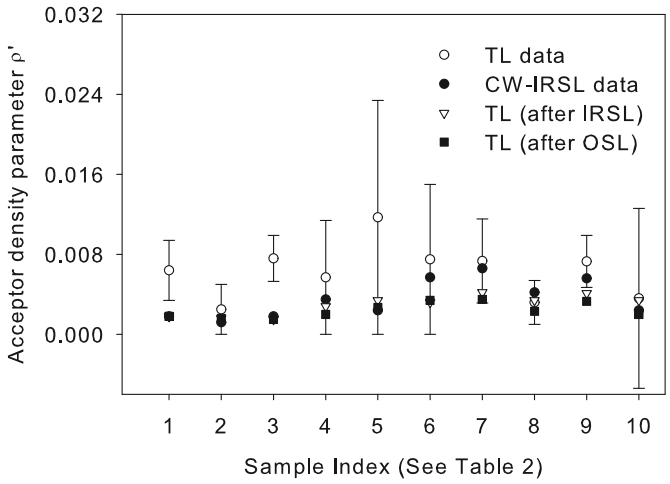

Fig. 7. Comparison of parameters from four different types of experiments, carried out on the 10 feldspars in Polymeris et al. [4]. The TL data (open circles) are from the deconvolution analysis in this paper, while the other three sets of data are from Sfampa et al. [5].

Fig. 8 shows typical results from analyzing 6 TL glow curves from samples J0994, J0995 and J0996. The labels J0994-1 and J0994-2 indicate two different aliquots of sample J0994. Fig. 8 shows that there are significant differences in the TL signals between the samples, but also between aliquots of the same sample. The number of optimal components N is indicated in each of the sub-figures in Fig. 8. Very good fits are obtained for all samples, with a compilation of the results from all $M = 24$ glow curves shown in Fig. 9 using radial plots.

Fifteen of the 24 glow curves required $N = 7$ components, two required $N = 8$, one required $N = 5$, and 6 required $N = 6$ components.

The conclusions from Fig. 9 are similar to those from Fig. 5, with all 24 values falling within the shaded $\pm 2\sigma$ bands. The relative standard error (RSE) for E_1, E_2, $ln(s)$ are again much smaller that the corresponding RSE for the dimensionless density parameter ρ'.

5.2. Deconvolution of CW-IRSL signals for bedrock samples

In this section deconvolution results are presented for the CW-IRSL signal from several of the feldspar samples studied by Brown and Rhodes [8] and Brown et al. [7]. The deconvolution requires two components based on the KP-CW Eq. (3), in order to fit accurately the experimental data. After irradiation, the samples are preheated for 60 s to 250 °C, before measurement of the CW-IRSL signal at 50 °C. It is assumed that the preheating process does not affect significantly the parameters describing the CW-IRSL signals. This assumption is based on several previous studies of CW-IRSL signals from feldspars, which showed that preheating of the samples affects minimally the shape of these signals (see for example Sahiner et al. [18], Jain et al. [20]).

A total of N = 28 CW-IRSL curves was analyzed, corresponding to 7 different doses administered to four different bedrock feldspars. The samples analyzed were two different aliquots for each of samples J0995 and J0999 in Table 3. Each of these aliquots was measured at 7 different doses of 30, 30, 60, 120, 240, 480 and 960 Gy. A typical CW-IRSL example for one of the 4 aliquots is shown in Fig. 10(a), measured at these 7 irradiation doses. Only the first 20 s of the signal are shown in Fig. 10(a), for purposes of clarity. The actual CW-IRSL signal being analyzed is 100 s long.

It was found that 9 of the 28 CW-IRSL curves could not be described reliably using the two components due to their low counts, and the results of the analysis for the remaining N = 19 CW-IRSL curves are shown in Fig. 10 in the form of radial plots.

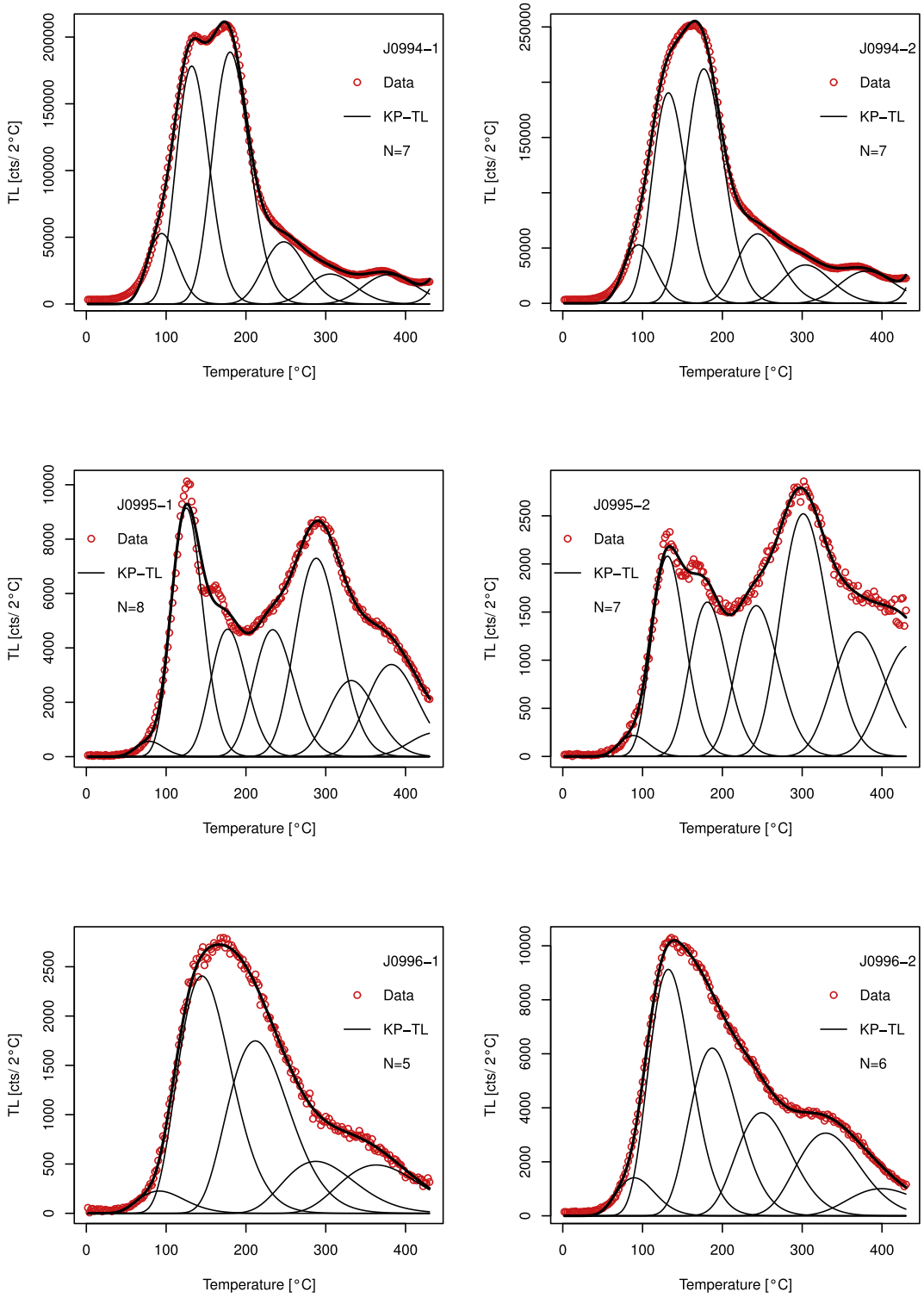

Fig. 8. Experimental TL glow curves from six representative laboratory irradiated bedrock samples, fitted using the Kitis-Pagonis analytical Eq. (1). The labels J0994-1 and J-0994-2 refer to two aliquots of the same sample J0994. The regenerative dose was 10 Gy. For more details on these samples, see Brown et al. ([7, 8]).

Fig. 10(b)–(d) show the radial plots for the best fit parameters A_1, A_2 and ρ'. Both the optical excitation rate A_1 and the density parameter ρ' show a low precision. In addition, 63% and 21% of the A_1 and ρ' values are located within the shaded $\pm 2\sigma$ area, while the respective percentage for the second optical excitation rate A_2 is 100%.

The average best fit parameters obtained from the least squares procedure applied to the N = 19 CW-IRSL curves are: density parameter $\rho' = 0.006 \pm 0.001$, optical excitation rates $A_1 = 19.2 \pm 0.02\ s^{-1}$ and $A_2 = 0.012 \pm 0.005\ s^{-1}$.

The average density parameter $\rho' = 0.006 \pm 0.001$ is in reasonable agreement with the average value of $\rho' = 0.011 \pm 0.004$ obtained from analyzing the N = 24 TL signals in the previous section.

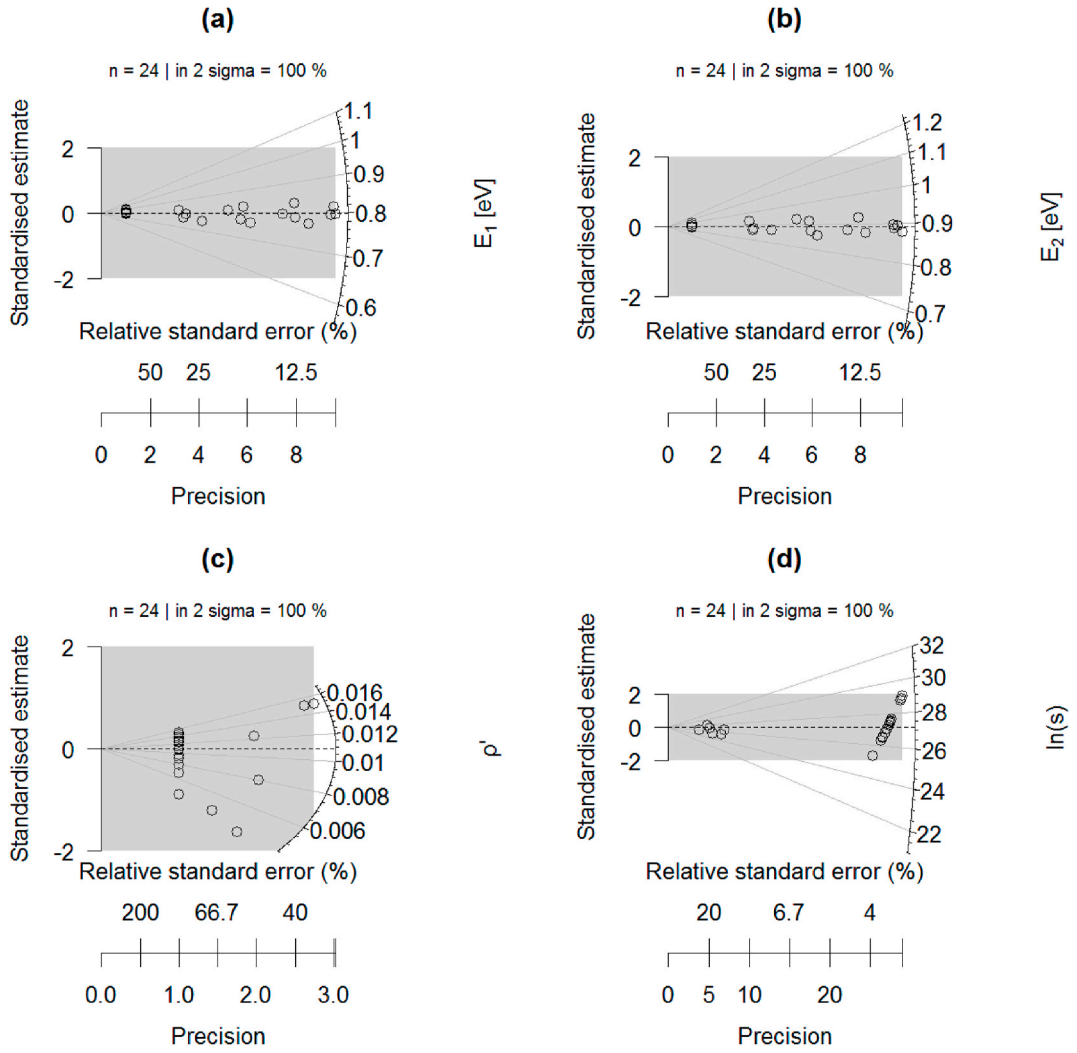

Fig. 9. Radial plots of the best fit parameters extracted from N = 24 laboratory irradiated bedrock samples, fitted using the Kitis-Pagonis analytical Eq. (1). For more details on the samples, see Brown et al. [7]. (a)–(b) Radial plots of the first two activation energy values E_1, E_2 (c) Radial plot of ρ' values (d) Radial plot of the frequency factors s.

5.3. Deconvolution of TL, CW-IRSL and LM-IRSL signals for sample J1000

Fig. 11 shows the deconvolution of the LM-IRSL signal from one of the feldspar samples studied by Brown and Rhodes [8] (Laboratory code J1000, a granodiorite gneiss). The deconvolution requires two components based on the KP-LM Eq. (5), in order to fit accurately the experimental data.

The best fit parameters from Fig. 11 are the optical excitation rates $b_1 = 0.58$ s^{-1} and $b_2 = 0.035$ s^{-1}, dimensionless density $\rho' = 0.012$, and amplitudes $I_1 = 1580$ ct/s, $I_2 = 582$ ct/s.

One of the feldspar samples studied by Brown and Rhodes [8] (Laboratory code J1000, a granodiorite gneiss), was chosen to carry out a comparative study of the deconvolution analysis of TL, CW-IRSL and LM-IRSL signals. After irradiation, the samples are preheated to 250 °C, before measurement of the LM-IRSL signal at 50 °C.

The results of the comparison are shown in Fig. 12. Fig. 12(a)–(c) show the deconvolution of the three signals, while Fig. 12(d) shows the results of measuring the LM-IRSL signals from three samples J0994, J1000 and J1002 (Table 3). In all cases, two LM-IRSL components were required to fit accurately the experimental data.

The best fit parameters obtained from the least squares procedure in the TL data of Fig. 12(a) are: density parameter $\rho' = 0.011 \pm 0.002$, frequency factor $s = 2.6 \times 10^{11}$ s^{-1}, $E_1 = 0.78$, $E_2 = 0.86$, $E_3 = 0.97$, $E_4 = 1.10$, $E_5 = 1.26$, $E_6 = 1.45$ eV.

The best fit parameters obtained from the least squares procedure in the CW-IRSL data of Fig. 12(b) are: density parameter $\rho' = 0.0100 \pm 0.0003$, optical excitation rates $A_1 = 12.4 \pm 0.2$ s^{-1} and $A_2 = 0.094 \pm 0.005$ s^{-1}

The best fit parameters are obtained from the least squares procedure in the LM-IRSL data of Fig. 12(c) are: excitation rates $b_1 = 0.58 \pm 0.06$ s^{-1} and $b_2 = 0.035 \pm 0.001$ s^{-1}, $\rho' = 0.012 \pm 0.001$.

The above three values of the density parameter for sample J1000 $\rho' = 0.011 \pm 0.002$, $\rho' = 0.0100 \pm 0.0003$ and $\rho' = 0.012 \pm 0.001$ are consistent with each other, within the precision of the fitting method. It is concluded that the three luminescence signals (TL, CW-IRSL and LM-IRSL) from sample J1000 can be described with a common value of the density parameter ρ'. The physical interpretation here is the presence of a common recombination center in the three luminescence processes.

6. Discussion and conclusions

In this paper it was shown that composite TL signals from feldspar samples of widely different provenance can be deconvoluted using the KP-TL analytical equation. All TL glow curves could be described in a uniform manner, as the superposition of several components

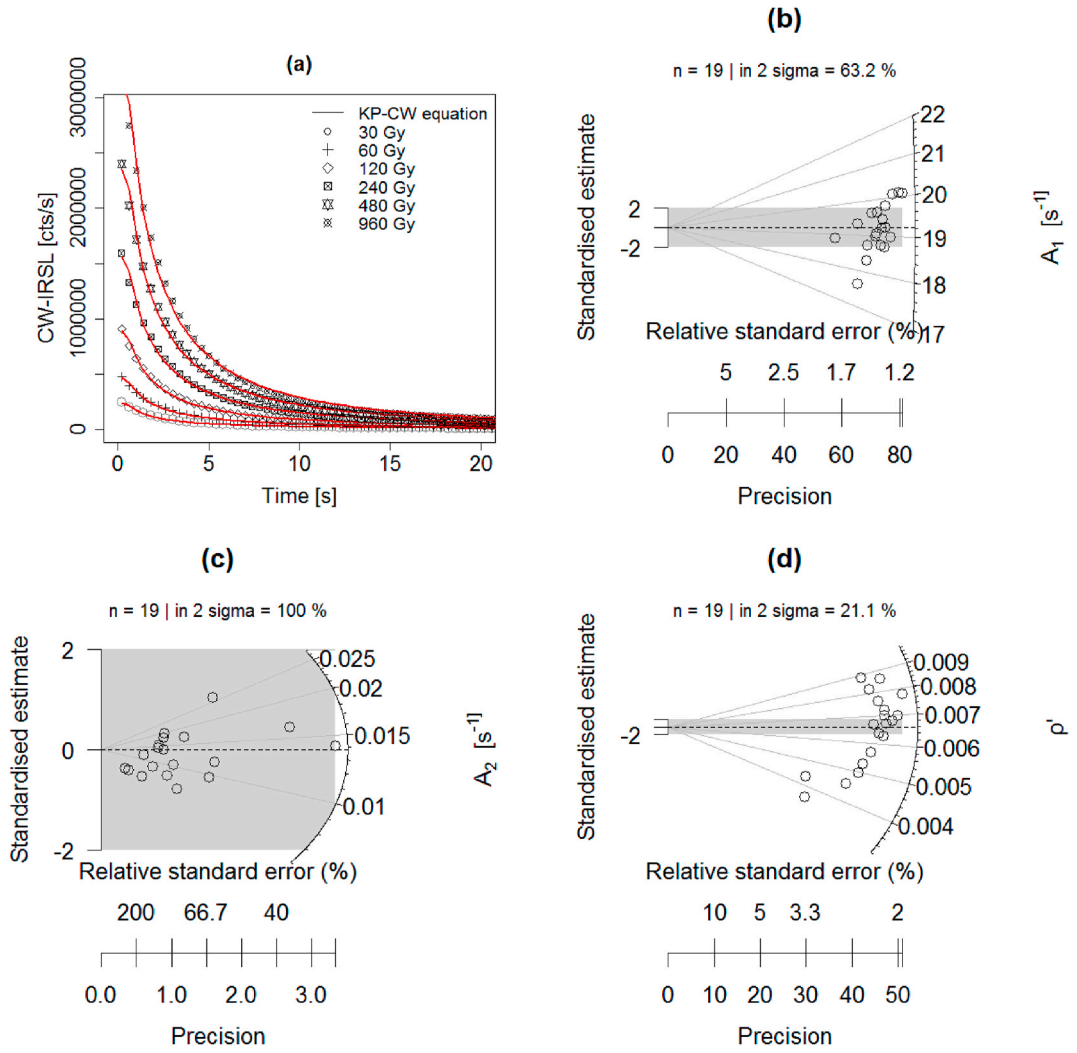

Fig. 10. (a) Deconvolution of CW-IRSL signal from a bedrock feldspar sample, measured after 7 different irradiation doses, using two components. (b)–(d) Radial plots of the best fit parameters A_1, A_2 and ρ' obtained by fitting a total of N = 19 CW-IRSL signals.

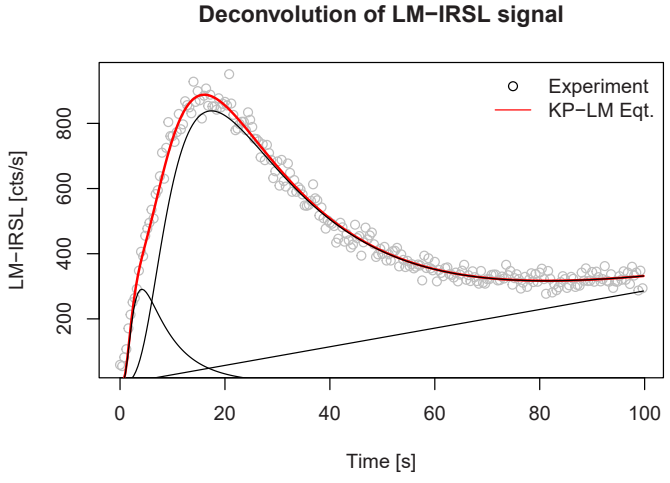

Fig. 11. Deconvolution of LM-IRSL signal for sample J1000. Two components are shown here, plus a linearly increasing background signal.

corresponding to distinct traps and a single recombination center. These signal components correspond to different activation energies and to the same frequency factor. All TL, CW-IRSL and LM-IRSL signals could be described by a narrow range of the dimensionless acceptor density parameter, consistent with previous analysis of these luminescence signals in the literature, which have concluded that these luminescence signals are likely to originate in a common recombination center.

It is perhaps surprising that this suite of naturally occurring alkali feldspar samples from Northern Greece and the Rocky Mountains of North America should share six activation energies and a narrow range of ρ' values, despite their different geologic histories, structural states (sanidine, orthoclase, microcline) and textures (high albite, perthite). An interesting question arising from this analysis is whether it is physically meaningful that six E values emerge. Kirsh et al. [27,28] attributed 5 to 8 unique E values derived from fractional glow curve analysis of albite and microcline samples to distinct emission bands associated with various traps accessing a common radiative recombination center. A more detailed discussion of feldspar TL spectral emission characteristics can be found in Krbetschek et al. [29], though only three emissions were identified in the blue detection window. Brokus et al. [30] noted that 42 feldspar samples across a wide geographical range exhibited the same characteristic cathodoluminescence spectral peaks, which can be associated with specific ion and defect sites. We suspect that a similar explanation applies here, though without corresponding spectral analysis, this is speculative.

In an extensive experimental study, Huntley and Lamothe [31] measured anomalous fading rates in K-feldspars separated from 49

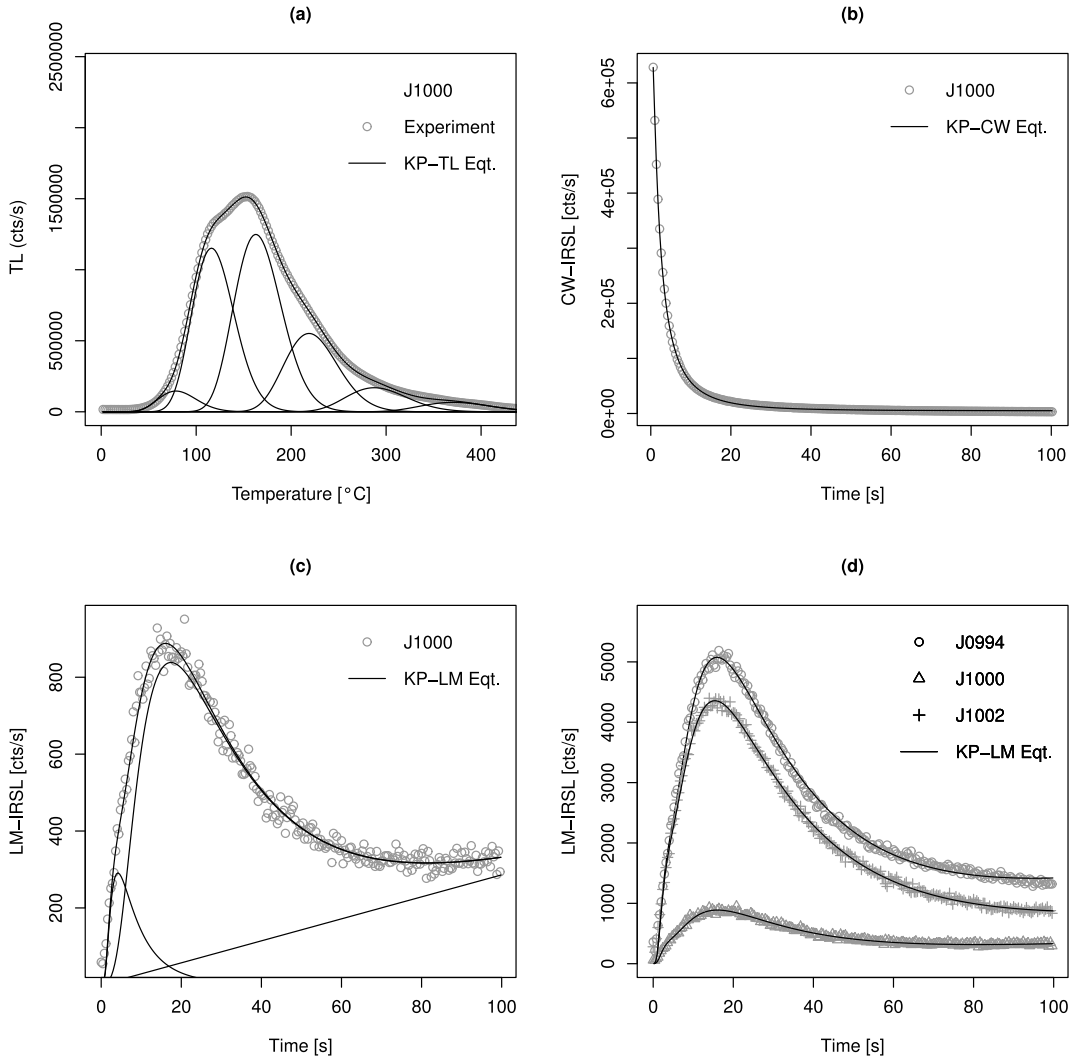

Fig. 12. Deconvolution of three types of signals for sample J1000. (a) TL signal (b) CW-IRSL signal (c) LM-IRSL signal (d) LM-IRSL fits for three different samples from Table 3 (J0994, J1000, J1002).

sediment samples, mainly from North America. These authors found that despite the very different provenances of these feldspar samples, anomalous fading was a ubiquitous phenomenon. In another comparative study, Pagonis et al. [15] studied the CW-IRSL signals from 23 museum samples and found that these signals could be described within a narrow range of the acceptor density parameter ρ'.

Recently Pagonis et al. [19] carried out a quantitative analysis of the TL glow curves for the 10 different samples listed in Table 1 of this paper, by using a Monte Carlo method and also a computerized deconvolution method based on the sum of Gaussian curves. The width of the Gaussian curves was found to be a common property characterizing all samples, at least within experimental error. In addition, the Gaussian width stayed practically unchanged when the irradiated samples underwent thermal treatments for different times and temperatures, or alternatively when they underwent optical bleaching treatments with blue LEDs.

In an important recent extensive experimental study, Riedesel et al. [32] explored the relationship between chemistry, structural state and the scale of exsolution of feldspar samples, based on their TL signals, emission spectra and IRSL fading rates. These authors obtained an estimate of 2.04 ± 0.05 eV for the optical trap depth, and a value of 1.44 ± 0.02 eV for the energy of the excited state of the IRSL trap. They tentatively concluded that the defects responsible for the IRSL signals in feldspar are within the aluminosilicate framework of feldspar; this framework is very similar for all alkali feldspars and this offers an explanation for the similarities of the feldspar luminescence characteristics.

The results from these detailed studies strongly suggest that TL and IRSL signals from feldspars exhibit common characteristics, and they can all be described with the mathematical techniques developed within the model of Jain et al. [3]. Specifically, the position and heights of the peaks in the TL glow curves from feldspars maintain a record of the thermal and optical history of the sample (Pagonis and Brown [33]), and the deconvolution method presented in this paper should be helpful for further development of thermochronometry applications using feldspar samples.

Finally, we wish to address under what experimental conditions one can use the KP-equations presented in this paper. These equations can be clearly used for prompt TL signals measured immediately after the end of the irradiation process in the laboratory. The museum feldspars by Polymeris et al. [4] were measured promptly, however the bedrock samples in this paper were measured by using a delay of 100 s after the end of irradiation. This was done in order to avoid a phosphorescence signal present in the low temperature region 0–50 °C. We estimate that the delay causes a reduction of the low temperature region 0–100 °C in the TL signal of the order of 5–10%, and should not affect drastically the parameters extracted using the least squares fitting method.

From a general point of view, one might expect that the kinetic pa-

rameters in a sample would remain unchanged when the sample is heated or optically stimulated in the laboratory. Specifically, the energy parameters E_i $(i = 1 \ldots N)$, the corresponding frequency parameter s and the density parameter ρ' should in principle stay unchanged for thermally/optically treated samples in the laboratory. However, the amplitudes of the TL components A_i $(i = 1 \ldots N)$ would be affected, and the sample would now be characterized by a truncated distribution of nearest neighbors. Several specific examples of such truncated distributions were given in the recent paper by Pagonis et al. [1]. The same type of problem is presented by the natural TL signals from field samples, since those would be also be described by a truncated NN distributions.

In principle then, the KP-equations would not be applicable *directly* to these treated and natural samples, however the kinetic parameters E_i, s_i and ρ' would still be the same as those extracted from analyzing the laboratory irradiated samples.

An interesting situation is presented by natural samples which are given an additive dose in the laboratory, as in a multiple aliquot additive dose protocol (MAAD). Our preliminary simulations show that the KP-equations should be directly applicable to the TL signals from such samples, as long as they are measured promptly after the end of the irradiation.

Clearly additional experiments and simulations are necessary in order to answer these rather complex questions.

7. Appendix: A distribution of activation energies *E*, or a distribution of frequency factors *s*?

One of the fundamental questions on TL signals from feldspars is whether one is dealing with a continuous distribution of energies E, a continuous distribution of frequency factors s, or perhaps with a combination of both possibilities. There are several published studies advocating for a continuous distribution of energy levels in K-feldspar (e.g. Garcia-Guinea et al. [34], Biswas et al. [35]), while other detailed experimental studies support the presence of a quasi-continuous distribution of energies consisting of closely overlapping distinct energy levels. For a more detailed description of several earlier studies on this topic, the reader is referred to the paper by Pagonis et al. ([36], Section 2).

In this Appendix we examine the simplest example of a trap characterized by an activation energy E and a frequency factor s, as described in the model of random defects of Jain et al. ([3,20]). The KP-TL equations used in this paper are the analytical solutions of this general model. Here it is demonstrated mathematically that within this model, the TL signal can be described in two physically different but equivalent ways, corresponding either to a distribution of energies E, or alternatively to a distribution of frequency factors s.

In the first subsection 7.1 below, the TL glow curve is described as the sum of several TL glow peaks, each with a different effective frequency factors $s_{\text{eff}}(r')$ corresponding to a different donor-acceptor distance parameter r', and a single activation energy E. In this first approach the energy E has a distinct value, and s is distributed.

In the second subsection 7.2, the TL glow curve is again described as the sum of several different TL glow peaks, each with a different effective activation energy $E_{\text{eff}}(r', T)$ corresponding to different distance parameter r' at each temperature T. In this second approach the frequency factor s has a single value, and E is distributed.

7.1. The TL glow curve as the sum of TL peaks with a distribution of frequencies

As discussed in Pagonis et al. [1], the intensity of the TL glow curve resulting from an excited state of the donor-acceptor pair in the model by Jain et al. [3] is obtained by integrating over both the dimensionless parameter distance r' and the time t, according to the equation:

$$I(t) = n_0 \int_{r'=0}^{\infty} 3(r')^2 \exp\left[-(r')^3\right] \exp\left[-s \exp\left[(\rho')^{-1/3} r'\right] \int_0^t e^{-E/kT} dt'\right] dr' \tag{10}$$

where n_0 (m^{-3}) is the total initial concentration of trapped charges, s (s^{-1}) is the frequency factor describing the TL process, E (eV) is the activation energy, ρ' and r' are respectively the dimensionless density and distance parameters describing the donor-acceptor system, k is the Boltzmann constant (eV K^{-1}), t (s) is the elapsed time during the TL measurement and T (K) is the temperature of the sample. The parameter s represents a total frequency factor describing the TL process in this model, and is an algebraic combination of three other frequency factors in the model (Pagonis et al. [1], page 10).

We now introduce an effective frequency factor $s_{\text{eff}}(r')$ given by:

$$s_{\text{eff}}(r') = s \exp\left[-(\rho')^{-1/3} r'\right] \tag{11}$$

and Eq. (10) becomes:

$$I(t) = n_0 \int_{r'=0}^{\infty} 3(r')^2 \exp\left[-(r')^3\right] \exp\left[-s_{\text{eff}}(r') \int_0^t e^{-E/kT} dt'\right] dr' \tag{12}$$

This equation can be interpreted as the sum of many constituent first order TL glow peaks; each peak corresponds to a different distance r', has an amplitude $3n_0 (r')^2 \exp\left[-(r')^3\right]$ which depends on the distance r', and has an effective frequency factor $s_{\text{eff}}(r')$ given by Eq. (11) (Pagonis et al. [37], Page 271).

Mathematically in this situation one is dealing with a single activation energy E, and a distribution of frequency factors $s_{\text{eff}}(r')$.

7.2. The TL glow curve as the sum of TL peaks with a distribution of energies

We can also describe the same TL curve by rewriting Eq. (10) as:

$$I(t) = n_0 \int_{r'=0}^{\infty} 3(r')^2 \exp\left[-(r')^3\right] \exp\left[-s \int_0^t \exp\left[-(\rho')^{-1/33} r'\right] e^{-E/kT} dt'\right] dr' \tag{13}$$

and by combining the exponential factors:

$$I(t) = n_0 \int_{r'=0}^{\infty} 3(r')^2 \exp\left[-(r')^3\right] \exp\left[-s \int_0^t \exp\left[-\frac{\text{kT}\,(\rho')^{-1/33} r' + \text{E}}{\text{kT}}\right] dt'\right] dr' \tag{14}$$

and by defining an effective energy $E_{\text{eff}}(r')$ as:

$$E_{\text{eff}}(r') = E + kT(\rho')^{-1/3} r' \tag{15}$$

we obtain:

$$I(t) = n_0 \int_{r'=0}^{\infty} 3(r')^2 \exp\left[-(r')^3\right] \exp\left[-s \int_0^t \exp\left[-\frac{E_{\text{eff}}(r')}{kT}\right] dt'\right] dr' \tag{16}$$

This equation can be interpreted as the sum of many constituent first order TL glow peaks; each peak corresponds to a different distance r', has an amplitude $3n_0 (r')^2 \exp\left[-(r')^3\right]$ which depends on the distance r',

and an effective activation energy $E_{eff}(r')$ given by Eq. (15). However, mathematically in this situation one is dealing with a single frequency factor s, and a distribution of energies $E_{eff}(r')$.

As a numerical example, consider a trap with $E = 1$ eV, $\rho' = 0.005$, $s = 10^{12}$ s^{-1}. These parameters result in a broad TL peak between 100 and 300 °C, with a maximum TL intensity around 170 °C. By using the range of physically meaningful values $r' = 0.1$–2.2 and the temperature of maximum intensity $T = 170$ °C, the effective energies can be calculated from Eq. (15) to be in the range $E_{eff}(r') = 1$–1.4 eV. This calculation shows that even in the simple situation of a single frequency factor $s = 10^{12}$ s^{-1}, the model results in an effective quasi-continuous distribution of energies in the range $E = 1$–1.4 eV.

In the same numerical example, the effective frequencies can be calculated from Eq. (11) to be in the range $s_{eff}(r') = 10^{9} - 10^{12}$ s^{-1} (even lower values of $s_{eff}(r')$ are physically possible, but they do not contribute significantly to the overall TL glow curve). This calculation shows that even in the situation of a single activation energy $E = 1$ eV, the model results in an effective quasi-continuous distribution of frequencies in the range $10^{9} - 10^{12}$ s^{-1}.

The TL glow curves calculated in *either* case of $E =$ constant or $s =$ constant are identical, since they are based on the same equation. However, the two *physical* descriptions of the process are different.

Declaration of competing interest

The authors declare that they have no known competing financial interests or personal relationships that could have appeared to influence the work reported in this paper.

References

[1] V. Pagonis, C. Schmidt, S. Kreutzer, Simulating feldspar luminescence phenomena using R, J. Lumin. 235 (2021) 117999, https://doi.org/10.1016/j.jlumin.2021.117999. URL, https://www.sciencedirect.com/science/article/pii/S0022231321001150.

[2] G. Kitis, V. Pagonis, Analytical solutions for stimulated luminescence emission from tunneling recombination in random distributions of defects, J. Lumin. 137 (2013) 109–115, https://doi.org/10.1016/j.jlumin.2012.12.042. URL, http://www.sciencedirect.com/science/article/pii/S0022231312007624.

[3] M. Jain, B. Guralnik, M.T. Andersen, Stimulated luminescence emission from localized recombination in randomly distributed defects, J. Phys. Condens. Matter 24 (38) (2012) 385402.

[4] G. Polymeris, E. Theodosoglou, G. Kitis, N. Tsirliganis, A. Koroneos, K. Paraskevopoulos, Preliminary results on structural state characterization of K-feldspars by using thermoluminescence, Mediterranean Archaeology and Archaeometry 13 (3) (2013) 155–161.

[5] I.K. Sfampa, G.S. Polymeris, V. Pagonis, E. Theodosoglou, N. Tsirliganis, G. Kitis, Correlation of basic TL, OSL and IRSL properties of ten K-feldspar samples of various origins, Nucl. Instrum. Methods Phys. Res. Sect. B Beam Interact. Mater. Atoms 359 (2015) 89–98, https://doi.org/10.1016/j.nimb.2015.07.106. URL, http://www.sciencedirect.com/science/article/pii/S0168583X15006849.

[6] I.K. Sfampa, G.S. Polymeris, V. Pagonis, G. Kitis, Correlation between isothermal TL and IRSL in K-Feldspars of various types, Radiat. Phys. Chem. 165 (2019) 108386, https://doi.org/10.1016/j.radphyschem.2019.108386. URL, https://www.sciencedirect.com/science/article/pii/S0969806X19305018.

[7] N.D. Brown, E.J. Rhodes, Thermoluminescence measurements of trap depth in alkali feldspars extracted from bedrock samples, Radiat. Meas. 96 (2017) 53–61, https://doi.org/10.1016/j.radmeas.2016.11.011.

[8] N. Brown, E. Rhodes, Dose-rate dependence of natural TL signals from feldspars extracted from bedrock samples, Radiat. Meas. 128 (2019) 106188, https://doi.org/10.1016/j.radmeas.2019.106188. URL, https://www.sciencedirect.com/science/article/pii/S1350448719304743.

[9] D.U. Wise, Laramide structures in basement and cover of the Beartooth uplift near Red Lodge, Montana, AAPG (Am. Assoc. Pet. Geol.) Bull. 84 (2000) 360–375.

[10] G.I. Omar, T.M. Lutz, R. Giegengack, Apatite fission-track evidence for Laramide and post-Laramide uplift and anomalous thermal regime at the Beartooth overthrust, Montana-Wyoming, GSA Bulletin 106 (1994) 74–85.

[11] E.J. Rhodes, Dating sediments using potassium feldspar single-grain IRSL: initial methodological considerations, Quat. Int. 362 (2015) 14–22, https://doi.org/10.1016/j.quaint.2014.12.012.

[12] L. Bøetter-Jensen, S. W. S. McKeever, A. G. Wintle, Optically Stimulated Luminescence Dosimetry, Elsevier Science, 2003.

[13] V. Pagonis, R. Chen, C. Kulp, G. Kitis, An overview of recent developments in luminescence models with a focus on localized transitions, Radiat. Meas. 106 (2017) 3–12, https://doi.org/10.1016/j.radmeas.2017.01.001. URL, http://www.sciencedirect.com/science/article/pii/S1350448717300094.

[14] V. Pagonis, Luminescence: Data Analysis and Modeling Using R, Use R!, Springer International Publishing, 2021. URL https://www.springer.com/us/book/9783030673109.

[15] V. Pagonis, M. Jain, K.J. Thomsen, A.S. Murray, On the shape of continuous wave infrared stimulated luminescence signals from feldspars: a case study, J. Lumin. 153 (2014) 96–103.

[16] I.K. Sfampa, G.S. Polymeris, N. Tsirliganis, V. Pagonis, G. Kitis, Prompt isothermal decay of thermoluminescence in an apatite exhibiting strong anomalous fading, Nucl. Instrum. Methods Phys. Res. Sect. B Beam Interact. Mater. Atoms 320 (2014) 57–63, https://doi.org/10.1016/j.nimb.2013.12.003. URL, http://www.sciencedirect.com/science/article/pii/S0168583X13011646.

[17] G. Kitis, G.S. Polymeris, E. Şahiner, N. Meriç, V. Pagonis, Influence of the infrared stimulation on the optically stimulated luminescence in four K-feldspar samples, J. Lumin. 176 (2016) 32–39, https://doi.org/10.1016/j.jlumin.2016.02.023. URL, http://www.sciencedirect.com/science/article/pii/S0022231315305846.

[18] E. Şahiner, G. Kitis, V. Pagonis, N. Meriç, G.S. Polymeris, Tunnelling recombination in conventional, post-infrared and post-infrared multi-elevated temperature IRSL signals in microcline K-feldspar, J. Lumin. 188 (2017) 514–523.

[19] V. Pagonis, G. Kitis, G.S. Polymeris, Quantum tunneling processes in feldspars: using thermoluminescence signals in thermochronometry, Radiat. Meas. 134 (2020) 106325, https://doi.org/10.1016/j.radmeas.2020.106325. URL, http://www.sciencedirect.com/science/article/pii/S1350448720300895.

[20] M. Jain, R. Sohbati, B. Guralnik, A.S. Murray, M. Kook, T. Lapp, A.K. Prasad, K. J. Thomsen, J.P. Buylaert, Kinetics of infrared stimulated luminescence from feldspars, Radiat. Meas. 81 (2015) 242–250, https://doi.org/10.1016/j.radmeas.2015.02.006. URL, http://www.sciencedirect.com/science/article/pii/S1350448715000335.

[21] J. J. Moré, The levenberg-marquardt algorithm: implementation and theory, in: G. A. Watson (Ed.), Numerical Analysis, Springer Berlin Heidelberg, Berlin, Heidelberg, 1978, pp. 105–116.

[22] R. Chen, V. Pagonis, Thermally and Optically Stimulated Luminescence: A Simulation Approach, John Wiley & Sons, Chichester, 2011.

[23] H.G. Balian, N.W. Eddy, Figure-of-merit (FOM), an improved criterion over the normalized chi-squared test for assessing goodness-of-fit of gamma-ray spectral peaks, Nucl. Instrum. Methods 145 (1977) 389–395, https://doi.org/10.1016/0029-554x(77)90437-2.

[24] A. Bluszcz, G. Adamiec, Application of differential evolution to fitting OSL decay curves, Radiat. Meas. 41 (7–8) (2006) 886–891.

[25] O.Q. De Clercq, J. Du, P.F. Smet, J.J. Joos, D. Poelman, Predicting the afterglow duration in persistent phosphors: a validated approach to derive trap depth distributions, Phys. Chem. Chem. Phys. 20 (2018) 30455–30465, https://doi.org/10.1039/C8CP06139D. URL https://doi.org/10.1039/C8CP06139D.

[26] M. Dietze, S. Kreutzer, M.C. Fuchs, C. Burow, M. Fischer, C. Schmidt, A practical guide to the R package Luminescence, Ancient TL 31 (2013) 11–18.

[27] Y. Kirsh, S. Shoval, P. Townsend, Kinetics and emission spectra of thermoluminescence in the feldspars albite and microcline, Phys. Status Solidi 101 (1987) 253–262.

[28] Y. Kirsh, N. Kristianpoller, S. Shoval, Kinetic analysis of natural and beta-induced TL in albite, Radiat. Protect. Dosim. 33 (1990) 63–66.

[29] M.R. Krbetschek, J. Götze, A. Dietrich, T. Trautmann, Spectral information from minerals relevant for luminescence dating, Radiat. Meas. 27 (1997) 695–748.

[30] S.A. Brokus, D.K. Silletti, J.M. Lunderberg, P.A. DeYoung, G.F. Peaslee, D. E. Carpenter, J. Buscaglia, Cathodoluminescence dependence on feldspar mineral structure and implications for forensic geology, Am. Mineral. 100 (2015) 451–458, https://doi.org/10.2138/am-2015-4461.

[31] D.J. Huntley, M. Lamothe, Ubiquity of anomalous fading in K-feldspars and the measurement and correction for it in optical dating, Can. J. Earth Sci. 38 (7) (2001) 1093–1106.

[32] S. Riedesel, A. Bell, G. Duller, A. Finch, M. Jain, G. King, N. Pearce, H. Roberts, Exploring sources of variation in thermoluminescence emissions and anomalous fading in alkali feldspars, Radiat. Meas. 141 (2021) 106541, https://doi.org/10.1016/j.radmeas.2021.106541. URL, https://www.sciencedirect.com/science/article/pii/S135044872100024X.

[33] V. Pagonis, N. Brown, On the unchanging shape of thermoluminescence peaks in preheated feldspars: implications for temperature sensing and thermochronometry, Radiat. Meas. 124 (2019) 19–28.

[34] J. Garcıa-Guinea, V. Correcher, A. Delgado, L. Sanchez-Munoz, Cluster linkages between luminescence emission spectra and continuous trap distribution in a volcanic sanidine, Radiat. Meas. 37 (4) (2003) 473–477, https://doi.org/10.1016/S1350-4487(03)00023-4. URL, https://www.sciencedirect.com/science/article/pii/S1350448703000234.

[35] R.H. Biswas, F. Herman, G.E. King, J. Braun, Thermoluminescence of feldspar as a multi-thermochronometer to constrain the temporal variation of rock exhumation in the recent past, Earth Planet Sci. Lett. 495 (2018) 56–68, https://doi.org/10.1016/j.epsl.2018.04.030.

[36] V. Pagonis, P. Morthekai, G. Kitis, Kinetic analysis of thermoluminescence glow curves in feldspar: evidence for a continuous distribution of energies, Geochronometria 41 (2014) 168–177, https://doi.org/10.2478/s13386-013-0148-z.

[37] V. Pagonis, J. Friedrich, M. Discher, A. Müller-Kirschbaum, V. Schlosser, S. Kreutzer, R. Chen, C. Schmidt, Excited state luminescence signals from a random distribution of defects: a new Monte Carlo simulation approach for feldspar, J. Lumin. 207 (2019) 266–272, https://doi.org/10.1016/j.jlumin.2018.11.024. URL, http://www.sciencedirect.com/science/article/pii/S0022231318317368.